Effect of Mesoporosity on Thermal and Mechanical Properties of Polystyrene/Silica Composites

Melissa A. Ver Meer,*,†,‡ Balaji Narasimhan,§ Brent H. Shanks,§ and Surya K. Mallapragada*,§

Schlumberger Lawrence Technology Center, Lawrence, Kansas 66049, Department of Materials Science and Engineering and Department of Chemical and Biological Engineering, Iowa State University, Ames, Iowa 50011

ABSTRACT In this study, mesoporous or colloidal silica particles were incorporated into polystyrene matrices via melt blending or by styrene polymerization initiated from the particle surface. The relationships between the surface morphology of filler particles in polymer composites and their thermomechanical properties were investigated. High molecular weight polystyrene−silica hybrids were generated by modifying the surfaces of monodisperse colloidal silica and templated mesoporous silica nanoparticles. The functionalized silica surfaces were grafted with alkyl halide initiators for atom transfer radical polymerization. Polymerization was conducted without free initiator present. The physical properties of these composites were studied by dynamic mechanical analysis, thermogravimetric analysis, transmission electron microscopy, and scanning electron microscopy. Results indicate that colloidal and mesoporous silica polymer composites generated by atom transfer radical polymerization have similar grafted polymer characteristics, indicating that polymer growth from the surface of the particle does not allow for significant polymer chain growth in the interior of the mesoporous silica particles.

KEYWORDS: polymer composites • atom transfer radical polymerization • melt blending • mesoporous silica • colloidal silica

INTRODUCTION

In polymer composite systems, the interfacial interactions between the polymer and the particles dictate the overall properties. Despite the wide array of inorganic particles available for composite preparation, two difficulties continually arise: (1) aggregation and (2) the lack of a strong interaction between the polymer matrix and filler. Dispersion of inorganic nanoparticles in a polymer is not easily achieved because nanoparticles have a strong tendency to agglomerate to reduce their surface energy, eliminating the potential benefit of the nanoscale filler. Recently, the introduction of mesoporous silica as reinforcement for polymer composites has generated great interest because of its potential to address the difficulties of both aggregation and interfacial interaction (1−7). Mesoporous silica has high specific surface area, uniform nanoscale pore sizes, and a high concentration of surface hydroxyl groups. Additionally, the interfacial interactions between the mesoporous silica and the polymer matrix can be improved through functionalization and grafting from the surface hydroxyl groups.

Processing conditions also influence interfacial interactions and aggregation within polymer composites. Polymer composites can be generated by melt blending of the particles in the polymer matrix, in situ sol−gel methods (8), or polymerization from particle surfaces. Melt blending of the filler particles into the polymer matrix is the simplest method of incorporating the inorganic component into the organic component, usually by polymer melt processing. Polymerization from the particle surface involves preparation of the surface as an initiator. The grafting step can then be conducted on the functionalized particle. There is a lack of direct comparisons between the properties of polymer composites generated by melt processing techniques and those prepared by grafting from the surface of the particle. The polystyrene-silica system was chosen as the model composite for this study, due to its relative ease of melt blending and the availability of established procedures for grafting polystyrene from the surface of colloidal silica (9−13).

In this work, we synthesized polymer composites with the inorganic phase based on mesoporous silica, as well as Stöber silica, by atom transfer radical polymerization (ATRP), allowing for a unique polymer−particle interface. High polymer brush density was required on the surface of the polystyrene-grafted silica particles to compare similar filler content between melt blended and grafted polymer composites. The mesoporous silica-based polymer composite could potentially clarify underlying relationships revolving around interfacial interactions of the polymer matrix and filler particles, as well as the structure and dependence of dispersion on the bulk properties including mechanical properties and thermal stability. Using this model system, we investigatedthese unique silica-based filler particles.

* To whom correspondence should be addressed. E-mail: mvermeer@slb.com (M.A.V.); suryakm@iastate.edu (S.K.M.).

Received for review August 12, 2009 and accepted December 5, 2009

† Schlumberger Lawrence Technology Center.

‡ Department of Materials Science and Engineering, Iowa State University.

§ Department of Chemical and Biological Engineering, Iowa State University.

DOI: 10.1021/am900540x

© 2010 American Chemical Society

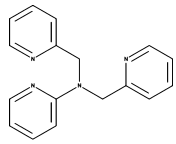

FIGURE 1. Trifunctional ligand, tris[(2-pyridyl)methyl]amine (TPMA).

EXPERIMENTAL SECTION

Materials. The filler particles used in this study consist both of the mesoporous silica, MCM-41, as well as its nonporous equivalent; spherical monodisperse colloidal silica generated using the Stöber method (14). The colloidal silica measured 470 nm in diameter. Mesoporous silica particles were prepared using a procedure developed by Deng et al. (15) to synthesize spherical MCM-41 particles with 360 nm diameters. They were characterized using scanning electron microscopy (SEM) (for surface morphology) and sorption experiments (for pore size characterization).

ATRP of Styrene from SiO_2 Colloidal and Mesoporous Initiators. In addition to the interface derived from the chemical interaction of the bulk polymer and the surface of the silica particles, it was desired to covalently bond the silica particles to the bulk polymer. This was achieved by preparing the surface of the silica particles to behave as initiators for ATRP synthesis of polystyrene. Using a relatively pH insensitive ligand (16), we grafted high-molecular-weight polystyrene polymer chains to the surface of both the colloidal and mesoporous silica. The grafting technique was a step-by-step process, allowing for the formation of the initiator on the surface of the particle.

Preparation of Polystyrene-Grafted Silica. Polystyrene-grafted Stöber and MCM-41 particles were prepared using a modified procedure from Nystrom et al. (17) The grafting technique first involved preparation of the Stöber and MCM-41 particles to accept the grafted PS chains prior to the polymerization.

The silica particles were dried under a vacuum at 60 °C for 24 h prior to use. The dried mesoporous silica particles (1.2 g) were added to a 250 mL round-bottomed flask containing 125 mL of anhydrous tetrahydrofuran (THF) (99.9%, Sigma-Aldrich) and 0.9 mL of 3-aminopropyltrimethoxysilane (APTMS) (97%, Aldrich) (0.9 mL). The solution was refluxed for 48 h at 65 °C. The particles were then separated from the reaction mixture via centrifugation and decanted. Fresh THF was added to the particles. The procedure was repeated four times to remove excess APTMS. The functionalized particles were dried under a vacuum at 60 °C for 24 h.

The 3-aminopropyltrimethoxy-functionalized silica particles were added to a round-bottomed flask containing 120 mL of dichloromethane (DCM) (99.8%, Sigma-Aldrich), 1.167 g of triethylamine (99.5% Aldrich), 2.232 g of 2-bromoisobutyrylbromide (98%, Aldrich), and a catalytic amount of 4-(dimethylamino)pyridine (DMAP) (99%, Aldrich). The reaction was quenched after 12 h by adding ethanol. The particles were separated from the reaction mixture via centrifugation and decanted, and fresh DCM was added. The decanting procedure was repeated four times. The 2-bromoisobutyrate functionalized particles were dried under a vacuum at 60 °C for 24 h.

Tris[(2-pyridyl)methyl]amine (TPMA) (Figure 1) was synthesized as described previously (18). The functionalized particles (313 mg) were added to 120 mg of TPMA, 30 mL of styrene (99%, Acros), 129 mg of elemental $copper_{(0)}$ (99%+, Fisher) and 13.6 mg of $copper_{(II)}$ bromide (Cu(II)Br) (98%, Aldrich) and immediately capped. The reaction temperature was carried out at 110 °C for 18.5 h. The grafted particles were diluted in chloroform and recovered by dropwise precipitation in methanol and subsequent filtration.

Preparation of Polystyrene–Silica Composites. The composites were prepared via extrusion melt intercalation. For comparison, commercial polystyrene (M_n = 84 000, M_w/M_n = 3.1, NOVA Chemicals Crystal PS 1510) was dried in a vacuum oven and stored in a desiccator prior to use. The PS 1510 was premixed with the Stöber or MCM-41 mesoporous silica particles (between 0.9 and 2.6% by wt.) and blended/extruded using a DSM Xplore 15 mL Microcompounder (Geleen, Netherlands) at 150 rpm at 190 °C for 2 min. The polystyrene-grafted particles were processed using the microcompounder under the same conditions without any additional polystyrene. The melt stream immediately entered a heated cylinder and transferred to the injection molder and molded into rectangular bars. Because of the residual stress present in the molded components, the rectangular bars were annealed under a vacuum above the glass-transition temperature at 177 °C. Samples were compressed into plaques at 177 °C.

Particle Characterization. Scanning electron microscopy (SEM) images were obtained using a JEOL JSA-840A SEM. The samples were prepared with carbon sticker mounting and a gold sputter coating of approximately 10–20 nm using a Denton Vacuum Desk II (Moorestown, NJ) sputter coating system. SEM images were used for silica particle size determination.

The PS composite samples were sectioned (70 nm) with a diamond knife on a Reichert Ultracut S ultramicrotome. Sections were collected onto copper grids and images obtained at 80 kV using a JEOL 1200 EXII scanning and transmission electron microscope (STEM) with a Megaview III digital camera and SIS Pro software.

The specific surface area of the silica particles was calculated by the Brunauer–Emmett–Teller (BET) method while pore size distribution was obtained from the Barrett–Joyner–Halenda (BJH) method.

Polystyrene Characterization. Gel permeation chromatography (GPC) data was carried out using a Waters 510 pump, Waters 717 autosampler, a Wyatt Optilab DSP refractometer and a Wyatt Dawn EOS light scattering detector. The mobile

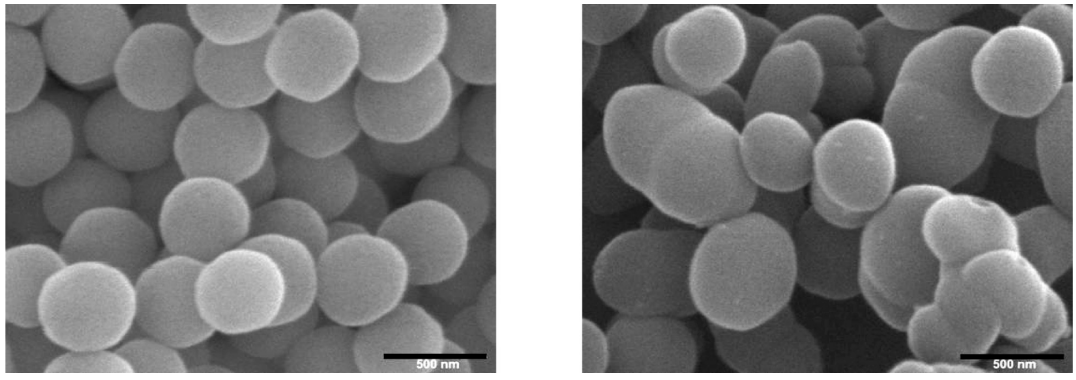

FIGURE 2. SEM images of Stöber, on the left, and mesoporous silica (MCM-41), on the right. Scale bars are 0.5 μm.

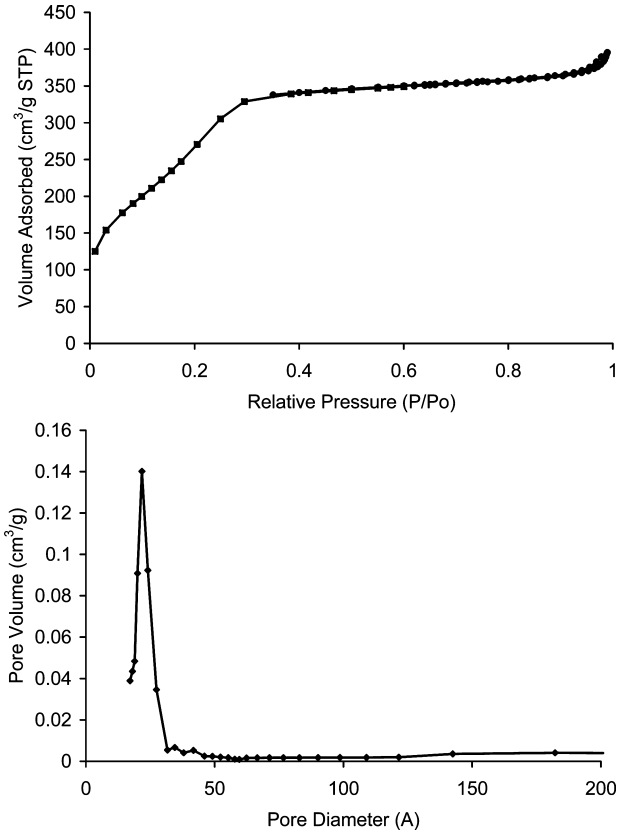

FIGURE 3. (Top) Adsorption−desorption isotherm of nitrogen at 77 K for MCM-41. (■ Adsorption, ● Desorption). (Bottom) BJH pore-size distribution plot from adsorption branch for MCM-41.

phase was THF at a flow rate of 1 mL/min. PS samples and standards were dissolved in THF at 1 mg/mL.

Thermal Properties. Thermogravimetric analysis (TGA) was conducted with a TA Instruments Q5000 (New Castle, DE). The materials were tested under a nitrogen atmosphere from 40 to 600 °C at 10 °C/min.

Mechanical Properties. Dynamic mechanical properties of the composites were measured using a TA Instruments Q800 Dynamic Mechanical Analyzer (DMA). Rectangular samples with dimensions of 2 × 7 × 18 mm^3 were used in a single cantilever bending mode. The experiments were carried out by varying the temperature from 30 to 150 °C at a heating rate of 1 °C/min, strain of 0.05% and frequency of 1 Hz.

RESULTS AND DISCUSSION

Silica Characterization. The morphologies of the colloidal and mesoporous silica were observed using SEM (Figure 2). Although the relative diameters of the two forms of silica particles are similar (470 nm diameter for Stöber particles and 360 nm for MCM-41 particles, as measured by scanning electron microscopy), the specific surface area for the mesoporous silica was 1031.9 m^2/g, as shown in Figure 3. In contrast, the surface area for Stöber silica was 8.2 m^2/g with no measured porosity. The mesoporous silica surface morphology allows for greater interaction with the polymer matrix based on the increased surface area. The surface interactions are also impacted by aggregation, which can control the mechanical properties of the final composite. Previous studies have indicated that silica particles should not be dried prior to polymerization to eliminate aggregation (19). However, because of the porous nature of mesoporous silica, it was determined that the silica particles would be dried to remove excess chemical species and solvents. The silica particles were dried but not calcined to minimize rigid aggregate formation.

Melt Blending. Colloidal and mesoporous silica particles were melt blended in polystyrene, creating polymer composites with spherical inorganic components of variable surface area. Melt processing via a twin screw extruder has been used to form polymer nanocomposites where layered silicates are dispersed in molten polymer (20). This technique eliminates the need for solvent and allows the polymer to diffuse from the bulk onto or into the surface of spherical silica particles. The TEM images in Figure 4 show individual mesoporous silica particle dispersion within the polystyrene matrix with the presence of large aggregates.

Initiator Grafting Density. Thermogravimetric analysis (TGA) was used to calculate the grafting density of the initiators, as shown in Figure 5, based on the method described by Save et al. (6) The weight loss between 30 and 200 °C was excluded, as it is due to physisorbed water on the silica surface (21). For the colloidal silica this constituted 1.97% and for the mesoporous silica this was 1.78% by

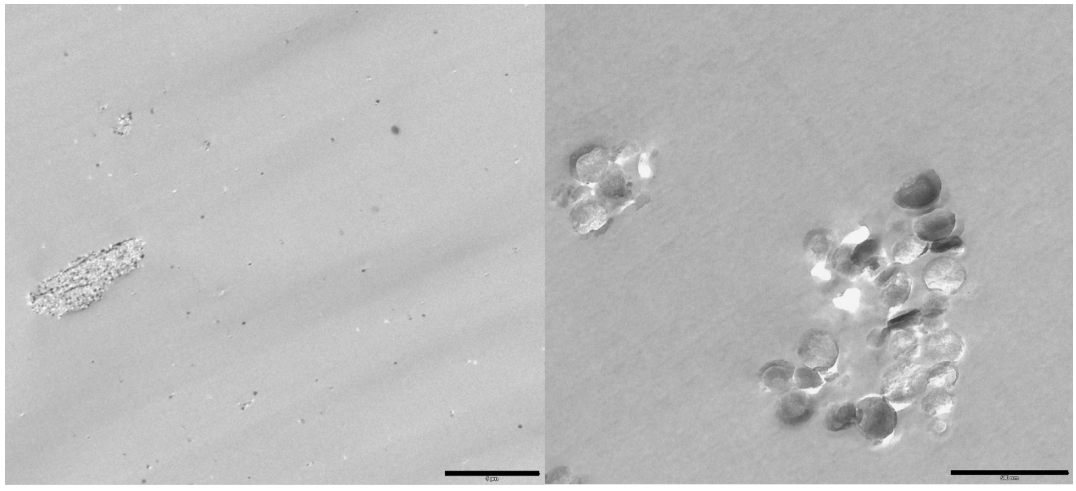

FIGURE 4. Polystyrene with MCM-41 incorporated, after melt compounding. Single particles present in polymer matrix with larger aggregates still present. Scale bars are 5 μm (left) and 0.5 μm (right), respectively.

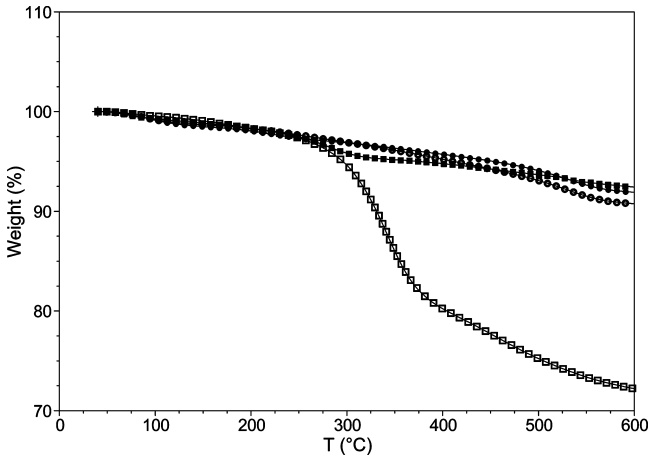

FIGURE 5. TGA thermograms of weight loss as a function of temperature. (● Stöber, ○ Br-grafted-Stöber, ■ MCM-41, □ Br-grafted-MCM-41).

weight. The weight loss between 30 and 600 °C was determined and the physisorbed water was subtracted from the total weight loss. The weight of initiator was 7.43% on the colloidal silica and 26.46% on the mesoporous silica, which amounts to 0.35 mmol of initiator grafted onto the colloidal silica and 1.28 mmol grafted onto the mesoporous silica per gram of sample.

The initiator grafting per gram of silica is nearly 4-fold for mesoporous silica versus colloidal silica, indicating that the interior pore space was indeed grafted with the ATRP initiator based on the weight loss indicated during the TGA tests. Although the number of potential initiator sites is significantly higher on the MCM-41 particles, the actual polymerization is remarkably similar to the monodisperse spherical silica of similar overall diameter as listed in Table 1. It appears that the growth of the polymer from the surface on the mesoporous silica prevents the interior pores from participating in the grafting process and the system behaves like spherical particles.

Silica Dispersion and Morphology. The ATRP results for the colloidal and mesoporous silica are shown in Table 1. TPMA was selected as a ligand based on temperature and pH stability for ATRP in the presence of limited amount of air (18). The use of TPMA resulted in fast polymerizations that initially gelled. Toluene was introduced to dilute the styrene and allow for high molecular weight ($>M_n = 150\,000$, $M_w/M_n < 1.3$) composites, which could then be compared to commercial polystyrene. As shown in Figure 6 and Figure 7, aggregation was minimized and single particle dispersion was prevalent. There was only slight improvement in the dispersion and aggregation between the polymer composites generated purely by blending versus the polymer composites generated by surface-initiated polymerization. The structure of the silica, relative to the amount of aggregation, was primarily determined prior to blending or polymerization processes.

Mechanical Behavior and Thermal Stability. DMA was used to measure the temperature dependence of the storage modulus (E'), loss modulus (E''), and loss factor (tan δ, E''/E'), varying both the surface morphology of the silica particles as well as the chemical interaction between the particle and the polymer matrix. Figure 8 shows the storage moduli of the colloidal and mesoporous silica-grafted

Table 1. Results for the ATRP Synthesis of Polystyrene−Silica[a]

sample	styrene	silica	$CuBr_2$[b]	TPMA	Cu(0)[b]	T (°C)[b]	t (h)[b]	$M_{n,GPC}$[b](g mol^{-1})	M_w/M_n[b]
SiO_2-g-PS	200	Stöber	0.030	0.1	1	110	18.5	156 868	1.29
M41-g-PS	200	MCM-41	0.030	0.1	1	110	18.5	240 805	1.30

[a] All polymerizations were performed in 50% (v/v) toluene. [b] $CuBr_2$ = copper(II) bromide; Cu(0) = elemental copper; T (°C) = reaction temperature; t (h) = reaction time; $M_{n,GPC}$ = average molar mass of grafted chains; M_w/M_n = polydispersity index.

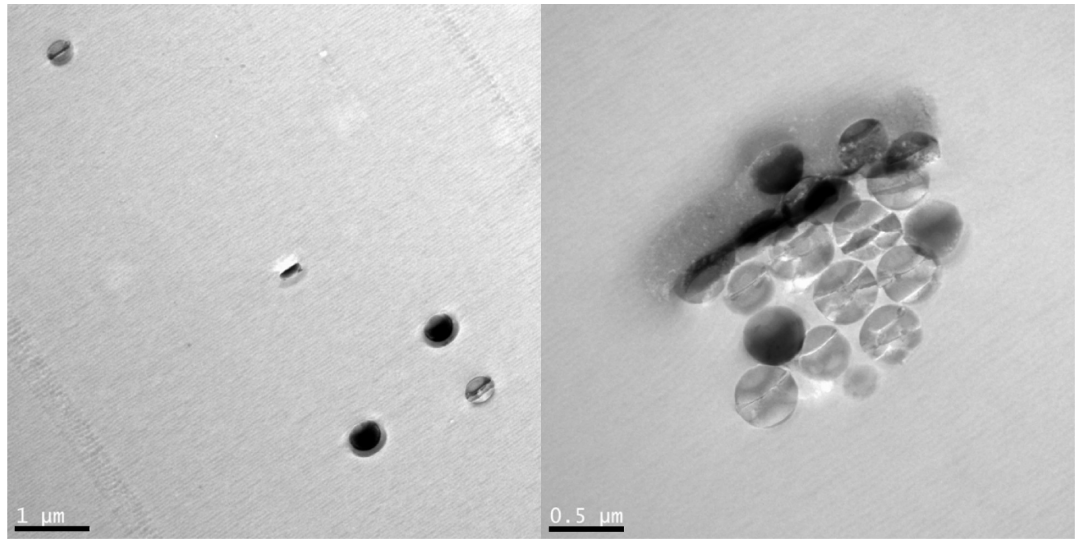

FIGURE 6. Polystyrene-grafted Stöber silica, after melt compounding. Single particles present in polymer matrix with smaller aggregates still present. Scale bars are 1 μm (left) and 0.5 μm (right), respectively.

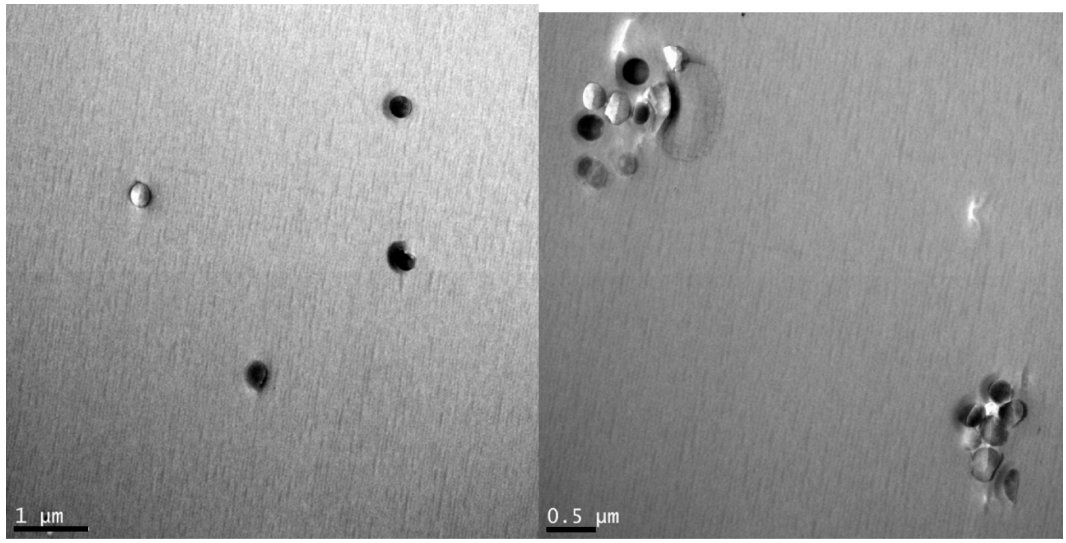

FIGURE 7. Polystyrene-grafted MCM-41 after melt compounding. Single particles present in polymer matrix with smaller aggregates still present. Scale bars are 1 μm (left) and 0.5 μm (right), respectively.

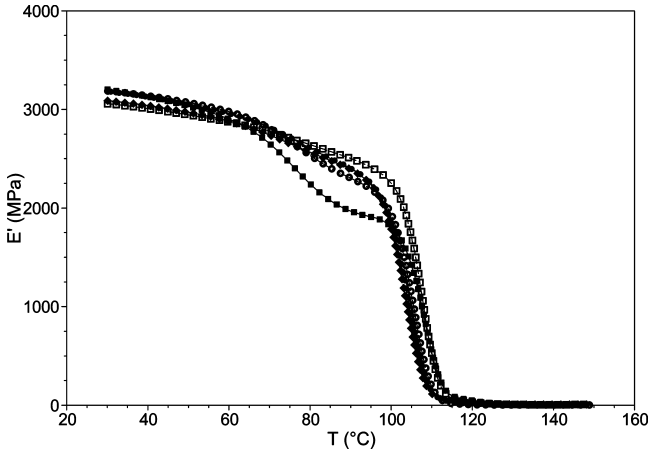

FIGURE 8. Storage modulus (E') as a function of temperature (■ SiO_2-g-PS, □ M41-g-PS, ◆ 0.9 SiO_2−PS, ● 2.6 SiO_2−PS, ○ 2.0 M41-PS).

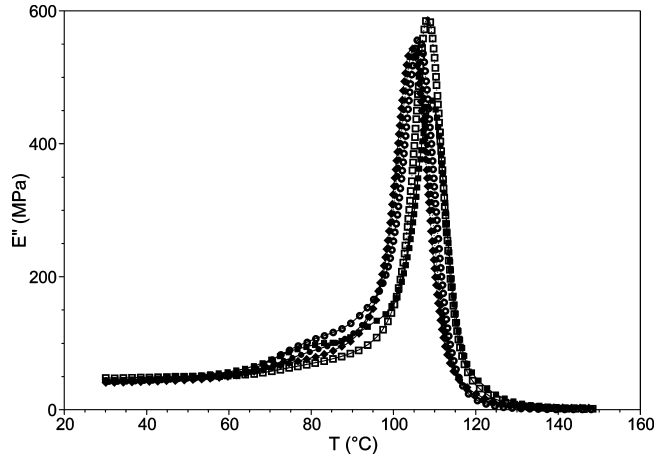

FIGURE 9. Loss modulus (E'') as a function of temperature (■ SiO_2-g-PS, □ M41-g-PS, ◆ 0.9 SiO_2−PS, ● 2.6 SiO_2−PS, ○ 2.0 M41-PS).

as well as the blended samples. The grafted mesoporous silica composites (open squares) show improved thermomechanical stability over the blended silica−polystyrene composites at high temperatures with the same inorganic content. This is consistent with the electron micrographs in Figure 7, which show single-particle dispersion and low aggregation. Interestingly, the SiO_2-g-PS composite shows two transitions, one with an onset at ∼63 °C and the second at ∼102 °C, which is the glass transition temperature. The M41-g-PS has only a slight discernible shift in storage modulus (E') at ∼65 °C and the glass transition onset is at ∼102 °C. The blended composites also showed small shifts at ∼65 °C. This shift at ∼65 °C is attributed to chain mobility, a behavior seen in other polymer−silica composite systems (1, 22, 23).

Glass-transition temperatures were 2−5 °C higher for the grafted particles versus the blended components based on the peaks of the loss modulus (E'') values, as shown in Figure 9. However, as shown in Figure 10, the blended mesoporous sample showed a dramatic increase in loss tangent (tan δ) as a function of temperature in comparison with other samples. This large tan δ is indicative of a material that will

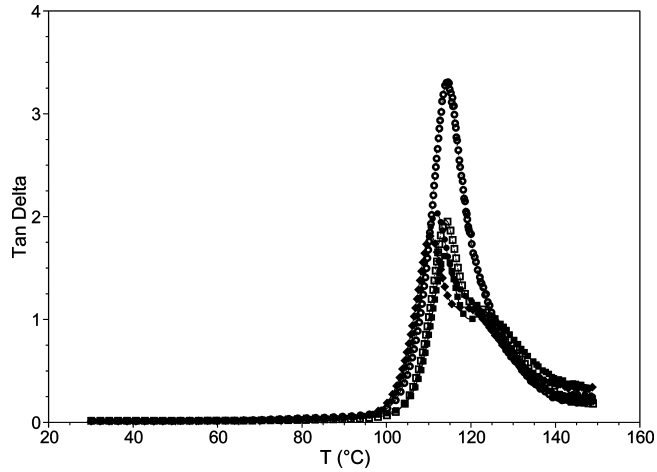

FIGURE 10. Loss tangent (tan δ) as a function of temperature (■ SiO_2-g-PS, □ M41-g-PS, ◆ 0.9 SiO_2−PS, ● 2.6 SiO_2−PS, ○ 2.0 M41-PS).

dissipate energy when stress is applied. Blending mesoporous silica into the polystyrene matrix results in an increased tan δ while maintaining the stiffness. This result also suggests that the blended and annealed mesoporous materials have an interpenetrating organic−inorganic network (24).

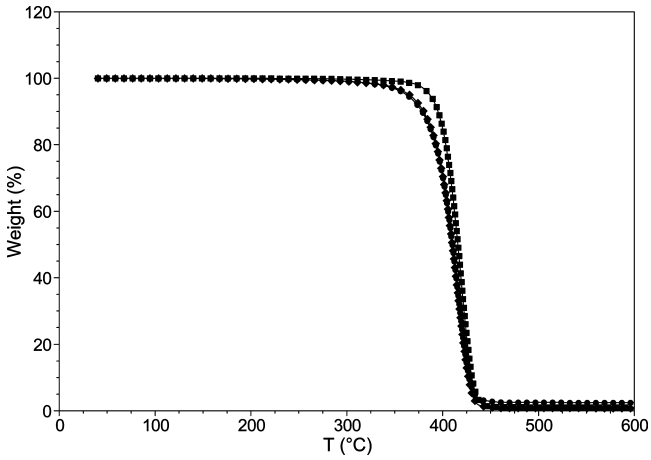

FIGURE 11. TGA thermograms of weight loss as a function of temperature (■ SiO_2-g-PS, ◆ 0.9 SiO_2-PS, ● 2.6 SiO_2-PS).

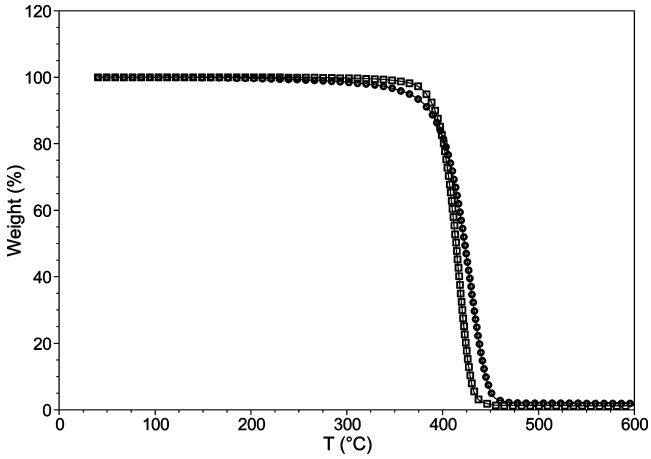

FIGURE 12. TGA thermograms of weight loss as a function of temperature (□ M41-g-PS, ○ 2.0 M41-PS).

In contrast, the M41-g-PS samples merely have the polystyrene chains adhered to the outer surface of the composites, resulting in a material with low dissipative energy. Interestingly, the potential penetration of the polystyrene into the pores of the melt blended and annealed polystyrene/mesoporous silica composite results in a material that has the potential to absorb more energy than comparable colloidal silica composites. Broadening the interfacial region appears to create a highly viscoelastic material.

Table 2. Sample Identification, Composite Preparation, and Relative Silica Loading Levels

sample	silica	preparation	wt % silica
SiO_2-g-PS	Stöber	graft	1.1
M41-g-PS	MCM-41	graft	1.3
0.9 SiO_2-PS	Stöber	blend	0.9
2.6 SiO_2-PS	Stöber	blend	2.6
2.0 M41-PS	MCM-41	blend	2.0

TGA studies for the polymer composites show enhanced thermal stability of the grafted composites in comparison to the blended composites. For the Stöber silica-based composites, the grafted sample did not lose 5 wt. % until 387 °C whereas the blended samples lost 5% of their weight between 363 and 365 °C, shown in Figure 11. As for the mesoporous silica-based composites, the grafted sample lost 5 wt % at 383 °C compared to 365 °C for the blended sample, as shown in Figure 12. Despite the relatively low filler loading, the presence of grafted versus unbound polystyrene resulted in a nearly 20 °C increase in degradation temperature. This is likely due to the fact that the polystyrene chain is bound on one surface and degradation occurs from the outer surface inward.

CONCLUSIONS

A customizable set of polymer composites was developed by employing either colloidal or mesoporous silica particles who surfaces were modified and used as initiators for ATRP of styrene. The grafted polymer composites were compared with conventional melt blended composites to study the

Scheme 1. Synthetic Approach for Polystyrene-Grafted Silica Particles by ATRP

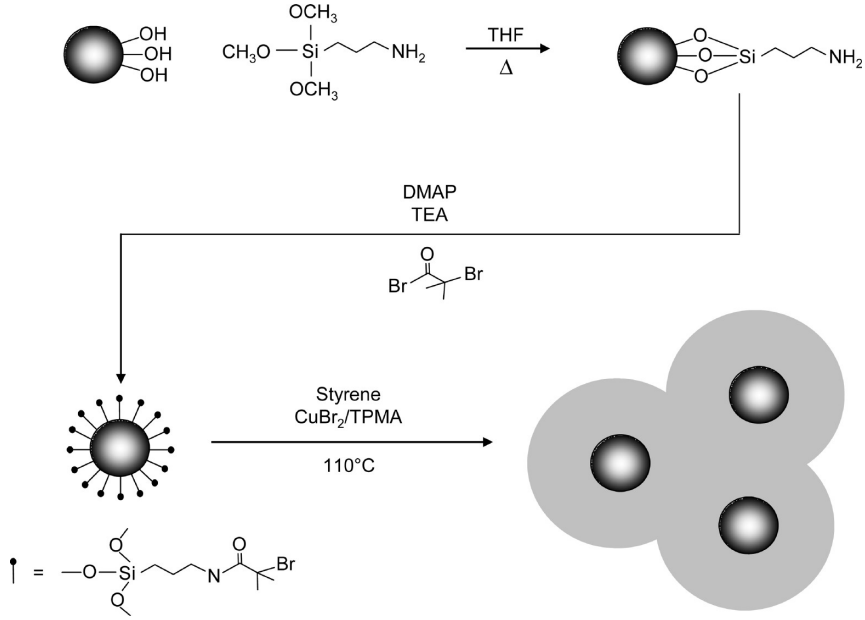

relationships between component properties, composition, structure, and interfacial interactions. Although the initiator grafting density was considerably higher for mesoporous silica versus colloidal spherical silica, the polymerization was limited to the accessibility of the initiator sites on the surface of the silica particles. It was demonstrated that the higher surface area inorganic component in mesoporous silica, as well as the covalently bonded polymer matrix and silica particles, increased the storage modulus and enhanced the thermal stability of the composites. These studies provide a basis for rationally designing composite materials based on polystyrene with controlled properties for specific applications.

Acknowledgment. This project was financially supported by Schlumberger Lawrence Technology Center. The authors thank Tracey E. Pepper (Iowa State University Bessey Microscopy Facility) and Warren Straszheim (Iowa State University Materials Analysis Research Laboratory) for their expert assistance with electron microscopy. Additionally, the authors thank Jason Holzmueller and Dr. William Goertzen of Schlumberger for thoughtful discussions.

REFERENCES AND NOTES

(1) Ji, X.; Hampsey, J. E.; Hu, Q.; He, J.; Yang, Z.; Lu, Y. *Chem. Mater.* **2003**, *15*, 3656–3662.
(2) He, J.; Duan, X.; Evans, D. G.; Howe, R. F. *J. Porous Mater.* **2002**, *9*, 49–56.
(3) Wang, N.; Li, M.; Zhang, J. *Mater. Lett.* **2005**, *59*, 2685–2688.
(4) Danumah, C.; Bousmina, M.; Kaliaguine, S. *Macromolecules* **2003**, *36*, 8208–8209.
(5) Danumah, C.; Ray, S. S.; Kaliaguine, S.; Bousmina, M. *J. Nanosci. Nanotechnol.* **2006**, *6*, 523–529.
(6) Save, M.; Granvorka, G.; Bernard, J.; Charleux, B.; Boissière, C.; Grosso, D.; Sanchez, C. *Macromol. Rapid Commun.* **2006**, *27*, 393–398.
(7) Audouin, F.; Blas, H.; Pasetto, P.; Beaunier, P.; Boissiere, C.; Sanchez, C.; Save, M.; Charleux, B. *Macromol. Rapid Commun.* **2008**, *29*, 914–921.
(8) Mark, J. E. *Polym. Eng. Sci.* **1996**, *36*, 2905–2920.
(9) Von Werne, T.; Patten, T. E. *J. Am. Chem. Soc.* **1999**, *121*, 7409–7410.
(10) Von Werne, T.; Patten, T. E. *J. Am. Chem. Soc.* **2001**, *123*, 7497–7505.
(11) Mori, H.; Seng, C. S.; Zhang, M.; Muller, A. H. E. *Langmuir* **2002**, *18*, 3682–3693.
(12) Savin, D. A.; Pyun, J.; Patterson, G. D.; Kowalewski, T.; Matyjaszewski, K. *J. Polym. Sci., Part B: Polym. Phys.* **2002**, *40*, 2667–2676.
(13) Liu, P.; Liu, W. M.; Xue, Q. J. *Eur. Polym. J.* **2004**, *40*, 267–271.
(14) Fox, J.; Kokoropoulos, P.; Wiseman, G.; Bowen, H. *J. Mater. Sci.* **1987**, *22*, 4528–4531.
(15) Deng, W.; Toepke, M. W.; Shanks, B. H. *Adv. Funct. Mater.* **2003**, *13*, 61–65.
(16) Matyjaszewski, K.; Jakubowski, W.; Min, K.; Tang, W.; Huang, J.; Braunecker, W.; Tsarevsky, N. *Proc. Natl. Acad. Sci. U.S.A.* **2006**, *103*, 15309–15314.
(17) Nystrom, D.; Antoni, P.; Malmstrom, E.; Johansson, M.; Whittaker, M.; Hult, A. *Macromol. Rapid Commun.* **2005**, *26*, 524–528.
(18) Tyeklar, Z.; Jacobson, R. R.; Wei, N.; Murthy, N. N.; Zubieta, J.; Karlin, K. D. *J. Am. Chem. Soc.* **1993**, *115*, 2677–2689.
(19) Ohno, K.; Morinaga, T.; Koh, K.; Tsujii, Y.; Fukuda, T. *Macromolecules* **2005**, *38*, 2137–2142.
(20) Vaia, R. A.; Ishii, H.; Giannelis, E. P. *Chem. Mater.* **1993**, *5*, 1694–1696.
(21) Vansant, E. F.; Van Der Voort, P.; Vrancken, K. C. *Characterization and Chemical Modification of the Silica Surface*, 1st ed.; Elsevier: Amsterdam, 1995, p 62—63.
(22) Forrest, J. A.; Dalnoki-Veress, K.; Dutcher, J. R. *Phys. Rev. E* **1997**, *56*, 5705–5716.
(23) Moller, K.; Bein, T.; Fischer, R. X. *Chem. Mater.* **1998**, *10*, 1841–1852.
(24) Run, M. T.; Wu, S. Z.; Zhang, D. Y.; Wu, G. *Mater. Chem. Phys.* **2007**, *105*, 341–347.

AM900540X